Hot and dense water in the inner 25 au of SVS13-A

C. Codella,[1]★ C. Ceccarelli,[2,3,1]★ E. Bianchi,[1,4]★ L. Podio,[1] R. Bachiller,[5]
B. Lefloch,[2,3] F. Fontani,[1] V. Taquet[6] and L. Testi[1,7]

[1]*INAF-Osservatorio Astrofisico di Arcetri, L.go E. Fermi 5, I-50125 Firenze, Italy*
[2]*Univ. Grenoble Alpes, IPAG, F-38000 Grenoble, France*
[3]*CNRS, IPAG, F-38000 Grenoble, France*
[4]*Dipartimento di Fisica e Astronomia, Università degli Studi di Firenze, I-50125 Firenze, Italy*
[5]*IGN, Observatorio Astronómico Nacional, Calle Alfonso XII, E-28004 Madrid, Spain*
[6]*Leiden Observatory, Leiden University, 9513, NL-2300-RA Leiden, The Netherlands*
[7]*ESO, Karl Schwarzschild Srt. 2, D-85478 Garching bei München, Germany*

ABSTRACT

In the context of the ASAI (Astrochemical Surveys At IRAM) project, we carried out an unbiased spectral survey in the millimetre window towards the well known low-mass Class I source SVS13-A. The high sensitivity reached (3–12 mK) allowed us to detect at least six HDO broad (full width at half-maximum $\sim$4–5 km s^{-1}) emission lines with upper level energies up to $E_u = 837$ K. A non-local thermodynamic equilibrium Large Velocity Gradient (LVG) analysis implies the presence of very hot (150–260 K) and dense ($\geq 3 \times 10^7$ cm^{-3}) gas inside a small radius ($\sim$25 au) around the star, supporting, for the first time, the occurrence of a hot corino around a Class I protostar. The temperature is higher than expected for water molecules are sublimated from the icy dust mantles ($\sim$100 K). Although we cannot exclude we are observing the effects of shocks and/or winds at such small scales, this could imply that the observed HDO emission is tracing the water abundance jump expected at temperatures $\sim$220–250 K, when the activation barrier of the gas phase reactions leading to the formation of water can be overcome. We derive $X(HDO) \sim 3 \times 10^{-6}$, and a H_2O deuteration $\geq 1.5 \times 10^{-2}$, suggesting that water deuteration does not decrease as the protostar evolves from the Class 0 to the Class I stage.

Key words: molecular data – stars: formation – ISM: molecules – radio lines: ISM – submillimetre: ISM.

1 INTRODUCTION

The origin of terrestrial water is still a source of intense debate (e.g. Ceccarelli et al. 2014; van Dischoeck et al. 2014; Altwegg et al. 2015). A key element to shed light on it, is how water evolves with time in proto-Sun analogues. Specifically, two aspects are particularly important: (1) the amount of water and its distribution in the planet formation region (a few tens of au) of the proto-Suns, and (2) its deuterium fractionation (e.g. Ceccarelli et al. 2014; Willacy et al. 2015).

With respect to the first point, water has been detected at all stages of the Sun-like star formation process, from pre-stellar cores and Class 0 sources to the Solar system (e.g. Ceccarelli et al. 1999; van Dishoeck et al. 2011, 2014; Caselli et al. 2012). However,

so far, we mostly have poor angular resolution observations that allowed us to detect the water emission, but not to resolve it on small ($\leq$1000 au) scales. Only a handful of observations exist with enough spatial resolution. They show that the water emission in the envelopes of Class 0 sources is concentrated in small regions, called hot corinos (Codella et al. 2010; Persson, Jørgensen & van Dishoeck 2013, 2014; Taquet et al. 2013; Coutens et al. 2014). On the contrary, no spatially resolved observations exist for the more evolved protostars, the Class I sources. With respect to the water deuterium fractionation, again only a few measures are available in Class 0 sources (Coutens et al. 2012, 2013, 2014; Persson et al. 2013, 2014; Taquet et al. 2013), but none in Class I.

In the context of the ASAI (Astrochemical Surveys At IRAM; http://www.oan.es/asai/) project, we have carried out a systematic study of the molecular emission towards SVS13-A. This is a well-studied young stellar object located in the NGC1333 star-forming region, at a distance of $\sim$235 pc (Bachiller et al. 1998; Hirota et al. 2008; Lee et al. 2016). SVS13-A is part of the system SVS13, where

three millimetre sources have been identified by interferometric observations (Bachiller et al. 1998; Looney, Mundy & Welch 2000), called A, B, and C. The distance between A and B is 15 arcsec, while C is 20 arcsec away from A. The systemic velocity of the sources A and B is between $+8\,km\,s^{-1}$ and $+9\,km\,s^{-1}$ (Chen et al. 2009; López-Sepulcre et al. 2015). The luminosity of SVS13-A has been estimated to be 34 $L_\odot$ (Chen et al. 2009; Tobin et al. 2016), where we corrected for the new estimate of the distance $d = 235$ pc (Hirota et al. 2008).

Although SVS13-A is still deeply embedded in a large-scale (~6000 au; e.g. Lefloch et al. 1998) envelope, its extended (>0.07 outflow pc) outflow, associated with the HH7-11 chain (e.g. Lefloch et al. 1998, and references therein), and its low L_{submm}/L_{bol} ratio (~0.8 per cent) lead to the classification as a Class I source (e.g. Chen et al. 2009 and references therein).

In this Letter, we report the detection of several lines of HDO towards SVS13-A, providing the first detection of deuterated water in a Class I source.

2 OBSERVATIONS

The present observations have been performed during several runs between 2012 and 2014 with the IRAM 30-m telescope near Pico Veleta (Spain) in the context of the ASAI[1] Large Program. In particular, the unbiased spectral surveys at 3 mm (80 116 GHz), 2 mm (129 173 GHz), and 1.3 mm (200 276 GHz) have been acquired using the EMIR receivers with a spectral resolution of 0.2 MHz. The observations were performed in wobbler switching mode with a throw of 180 arcsec towards the coordinates of the SVS13-A object, namely $\alpha_{J2000} = 03^h29^m03\overset{s}{.}29$, $\delta_{J2000} = +31°16'03\overset{''}{.}8$. The pointing was checked by observing nearby planets or continuum sources and was found to be accurate to within 2–3 arcsec. The Half Power Beam Widths (HPBWs) are in the 9–31 arcsec range.

The data were reduced with the GILDAS–CLASS[2] package. Calibration uncertainties are ≃10 per cent at 3 mm and ~20 per cent at shorter wavelengths. All the spectra have been converted from antenna temperature to main beam temperature (T_{MB}), using the main beam efficiencies reported on the IRAM 30-m website.[3]

3 RESULTS AND DISCUSSION

3.1 HDO detected lines

The ASAI unbiased survey allows us to detect seven HDO lines (1 in the 3 mm band, 1 in the 2 mm band, and 5 in the 1.3 mm one) covering a wide range of excitation, with upper level energies E_u from 47 to 837 K. The 81 GHz line is only tentatively detected, given the low S/N ratio. However, the following analysis will show how the $1_{1,0}-1_{1,1}$ intensity is well in agreement with those of the other lines observed at 2 and 1.3 mm. The $3_{3,1}-4_{2,2}$ transition (at ~242.0 GHz) is the HDO line with the highest upper level energy ($E_u = 837$ K) ever observed towards a low-mass protostar. The profiles of all detected lines are shown in Fig. 1, while Table 1 reports the results of the line Gaussian fits. The HDO emission peaks at the cloud systemic velocity, between $+8.0$ and $+9.0\,km\,s^{-1}$ (Chen et al. 2009; López-Sepulcre et al. 2015). The lines are quite broad, with an FWHM ~ $4.2–4.9\,km\,s^{-1}$ for all the lines but the two observed
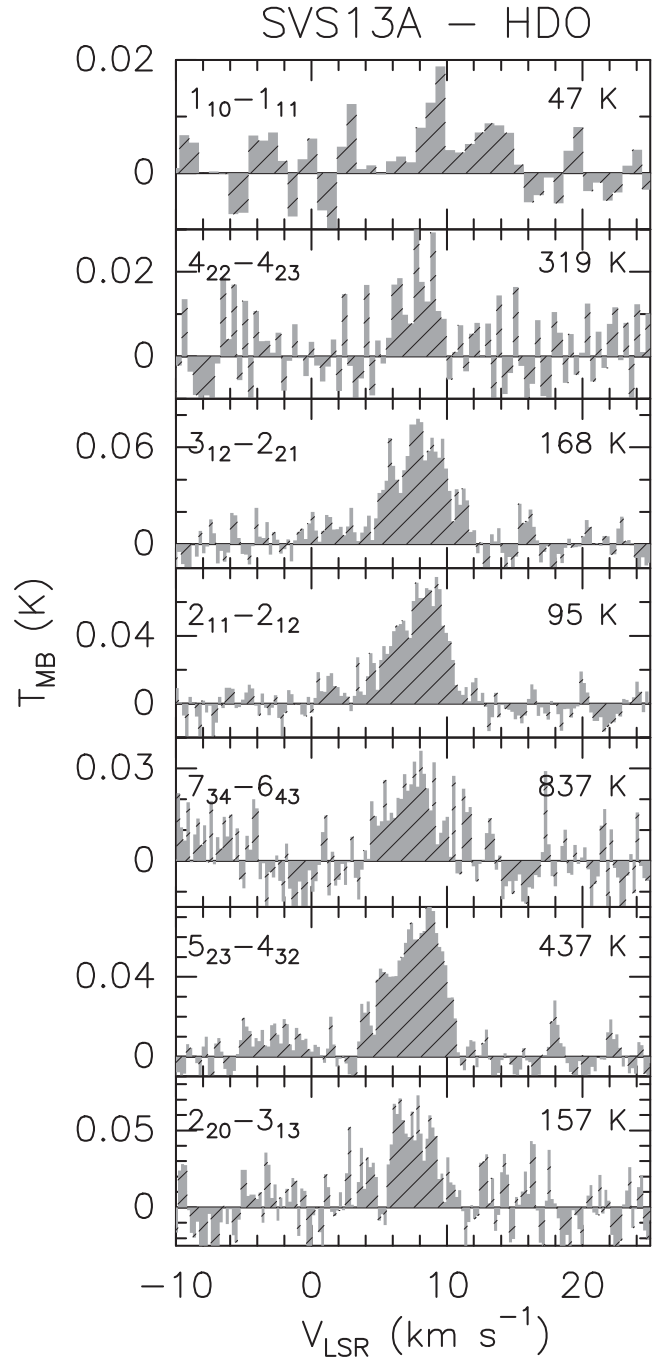
Figure 1. HDO line profiles (in main-beam temperature, T_{MB}, scale) observed with the IRAM 30-m antenna towards SVS13-A. In each panel, both the transition and the upper level energy, E_u, are reported.

at 3 and 2 mm, which are also those observed with the lowest S/N ratio and the worst spectral resolution (from 0.7 to 0.2 $km\,s^{-1}$ moving from 80.6 and 266.2 GHz). The emission in the 1 and 2 mm bands only originates from SVS13-A, as SVS13-B, 15 arcsec southwest, is outside the *HPBW*. The 3 mm band might, in principle, contain some emission from SVS13-B. However, the analysis of the measured fluxes tends to exclude a substantial contamination from SVS13-B also in this band (see below).

Finally, we searched for $H_2^{18}O$ lines in our spectral survey and found none. The most sensitive upper limit to the H_2O column density is set by the non-detection of the para–$H_2^{18}O$ $3_{1,3}-2_{2,0}$ line

Table 1. List of HDO transitions and line properties (in T_{MB} scale) detected towards SVS13-A.

Transition	ν^a (GHz)	HPBW[a] (arcsec)	$g_u{}^a$	$E_u{}^a$ (K)	$S\mu^{2a}$ (D^2)	$\log(A/s^{-1})^a$	rms (mK)	$T_{peak}{}^b$ (mK)	$V_{peak}{}^b$ (km s^{-1})	FWHM[b] (km s^{-1})	$I_{int}{}^b$ (mK km s^{-1})
$1_{1,0}-1_{1,1}$	80.578 29	31	3	47	0.66	−5.88	5	14(2)	+9.2(0.3)	1.7(0.9)	26(9)
$4_{2,2}-4_{2,3}$	143.727 21	17	9	319	0.73	−5.55	9	21(8)	+8.0(0.3)	3.1(0.8)	68(20)
$3_{1,2}-2_{2,1}$	225.896 72	11	7	168	0.69	−4.88	7	45(7)	+8.0(0.1)	4.9(0.3)	234(16)
$2_{1,1}-2_{1,2}$	241.561 55	10	5	95	0.36	−4.92	6	41(6)	+8.0(0.1)	4.7(0.3)	206(9)
$7_{3,4}-6_{4,3}$	241.973 57	10	15	837	1.39	−4.82	7	17(5)	+7.7(0.3)	4.6(0.7)	83(10)
$5_{2,3}-4_{3,2}$	255.050 26	10	11	437	1.02	−4.75	6	40(6)	+7.8(0.1)	4.5(0.2)	199(9)
$2_{2,0}-3_{1,3}$	266.161 07	9	5	157	0.40	−4.76	12	31(9)	+7.4(0.3)	4.2(0.8)	141(19)

[a]From the Jet Propulsion Laboratory data base (Pickett et al. 1998).
[b]The errors are the Gaussian fit uncertainties.

at 203.407 52 GHz.[4] We obtained a 3σ upper limit on the peak temperature (in T_{MB} scale) of 20 mK.

3.2 Analysis of the HDO emission

We analysed the observed HDO line emission with the non-local thermodynamic equilibrium (LTE) Large Velocity Gradient (LVG) model by Ceccarelli et al. (2003), using the collisional coefficients for the system HDO-H_2 computed by Faure et al. (2012) and extracted from the BASECOL data base (Dubernet et al. 2013). We assumed a plane-parallel geometry and a Boltzmann distribution for the ortho-to-para H_2 ratio of 3. Note that the collisional coefficients with ortho-H_2 can be a factor 5 larger than the corresponding coefficients with para-H_2 (Faure et al. 2012), but only at low temperatures ($\ll$45 K) and not at those here discussed (see below). Note also that the HDO $7_{3,4}-6_{4,3}$ line (with $E_u = 837$ K) has been excluded from the LVG analysis because the corresponding collisional rates have not been calculated (see later for a comparison with an LTE approach).

We run a large grid of models varying the temperature T_{kin} from 100 to 300 K, the H_2 density n_{H2} from 8×10^8 to 1×10^{10} cm^{-3}, the HDO column density $N(HDO)$ from 4×10^{16} to 7×10^{17} cm^{-3}, and the emitting sizes θ_s from 0.05 to 10 arcsec. The lowest χ_r^2 is obtained with $N(HDO) = 4 \times 10^{17}$ cm^{-2}, and $\theta_s = 0.2$ arcsec, corresponding to $\sim$50 au. Fig. 2 (upper panel) shows the χ_r^2 contour plot as a function of the temperature and H_2 density with these values. The best-fitting solution is found for a very high temperature, $T_{kin} = 150$–260 K, and a quite high density $n_{H_2} \geq 3 \times 10^7$ cm^{-3}. Fig. 2 (lower panel) shows the goodness of the fit, namely the ratio between the measured velocity-integrated intensities and the LVG model predictions, as a function of the line upper level energy, for the best-fitting solution: $N(HDO) = 4 \times 10^{17}$ cm^{-2}, $\theta_s = 0.2$ arcsec, $T_{kin} = 200$ K, and $n_{H_2} = 2 \times 10^8$ cm^{-3}. The lines are predicted to be optically thin to moderately thick. The largest opacities are $\sim$2 for the four lowest lying lines (at 80.58, 241.56, 266.16 and 225.90 GHz), while the other lines have opacities lower than unity.

Finally, the populations of the detected transitions are predicted to be close to LTE. Indeed, since non-LTE predictions were not possible for the higher lying line at 241.97 GHz, we also computed the LTE solution (see Fig. 3), finding a rotational temperature of 334 ± 42 K, which is larger than the kinetic temperature derived from the LVG analysis, i.e. 160–240 K considering the 1σ χ_r^2 solution. In practice, assuming the non-LTE LVG solution,

[4] From Jet Propulsion Laboratory data base, http://spec.jpl.nasa.gov/home.html; Pickett et al. (1998).
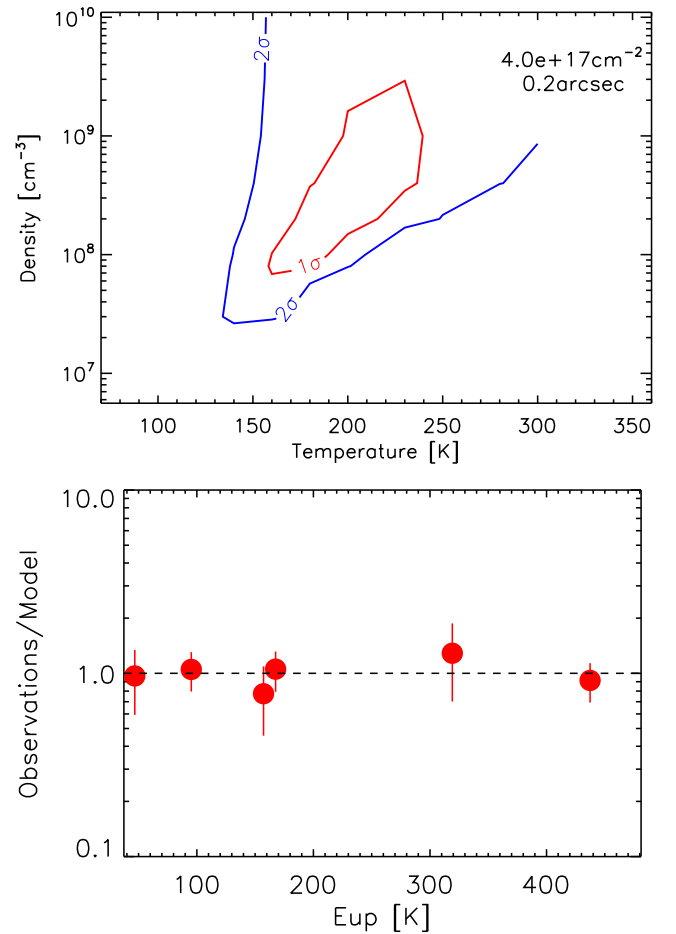

Figure 2. Upper panel: the χ_r^2 contour plot obtained considering the non-LTE model predicted and observed intensities of all detected HDO lines but the 241.974 GHz line with $E_u = 837$ K (for which no collisional rates are available). The best fit is obtained with 0.2 arcsec, $N_{HDO} = 4 \times 10^{17}$ cm^{-2}, $T_{kin} = 200$ K, and $n_{H_2} = 2 \times 10^8$ cm^{-3}. The 1σ and 2σ of the χ_r^2 contours are reported. Lower panel: ratio between the observed line intensities with those predicted by the best-fitting model as a function of line upper level energy E_u.

the agreement between the predicted and observed intensity of the $E_u = 857$ K is within a factor 2; this is acceptable if we consider the opacity of the low-E_u lines and that the LTE condition may not apply to such a high lying line so that we cannot exclude a temperature gradient with a component with T_{kin} larger than 200 K. High spatial resolution observations are required to clarify this point.
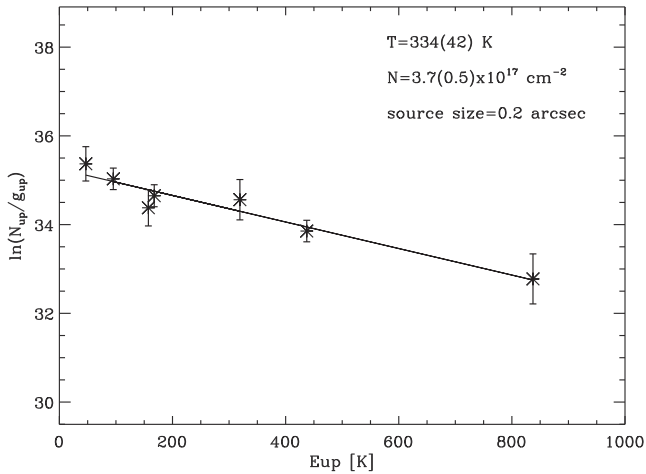
Figure 3. Rotation diagram for the HDO transitions reported in Table 1, including the $E_{up} = 837$ K, not considered in the LVG analysis (see Fig. 2). The parameters N_{up}, g_{up}, and E_{up} are, respectively, the column density, the degeneracy, and the energy of the upper level. The error bars on $\ln(N_{up}/g_u)$ are given by the vertical bar of the symbols. The plot allows us to derive a rotational temperature of 334 ± 42 K and a total column density of $3.7 \pm 0.5 \times 10^{17}$ cm^{-2}.

3.3 Origin of the HDO emission

The non-LTE analysis reveals the presence of a hot (150–260 K), dense ($\geq 3 \times 10^7$ cm^{-3}) and compact ($\sim$50 au) component in SVS13-A. Note that the density estimate well agrees with that derived from dust continuum by Chen et al. (2009). High temperatures (218 K) have been similarly obtained by Coutens et al. (2014) applying an LTE analysis to four HDO lines detected, using the PdB array, towards the Class 0 NGC1333 IRAS2A. Also, high excitation conditions have been found through LVG analysis of H_2O lines as observed by *Herschel* towards both Class 0 and Class I sources (e.g. Herczeg et al. 2012; Podio et al. 2012; Karska et al. 2013; Busquet et al. 2014; Kristensen et al. 2016); in these cases, the high excitation H_2O emission has been associated with shocked gas induced by jets. Thus, the present results may indicate the presence of jet-induced shocks on the $\sim$20 au scales. However, the jet hypothesis is ruled out by: (i) the full width at half-maximum (FWHM) line profiles ($\simeq 4$ km s^{-1}, the is usually traced by velocities larger than 10 km s^{-1}), and (ii) the compact size inferred by the LVG analysis. On the other hand, HDO emission could be emitted by shocks induced by the viscosity of a disc or it could probe the base of a disc wind (as suggested by Codella et al. 2016 for the Class 0 HH212). Again, there is no signature in the line profile suggesting an association of water with a small portion of the large discs expected to be around Class I objects (around 250 au; e.g. Eisner 2012).

In conclusion, what is HDO tracing in the SVS13-A system? The observed high temperature and linewidth are consistent with *the presence of a hot corino* inside SVS13-A, where the gas is thermally heated by the central source. Of course, the definition of hot corino involves the detection of complex organic molecules (e.g. Ceccarelli et al. 2007). We anticipate that this is indeed the case for SVS13-A (Bianchi et al., in preparation). Assuming that the dust is heated by the 34 L$_\odot$ central source and that the dust emission is optically thin, the dust temperature would be about 200 K at a distance of $\sim$25 au (see e.g. Ceccarelli et al. 2000, equation 1). Of course, if the dust opacity is thick in the innermost regions, then this value is a lower limit. Therefore, this temperature is in good agreement with the LVG analysis. Indeed, high temperatures

from HDO were observed by Coutens et al. (2014) towards the Class 0 object NGC1333-IRAS2A, in agreement with the present hypothesis that HDO lines, being optically thin, probe inner regions around the protostars.

However, the hot corino interpretation has a problem. If the high temperature is caused by the thermal heating, one would expect that water is sublimated from the icy grain mantles at $\sim$100 K, whereas the HDO line emission indicates a larger temperature. Why? A first possibility could be that the HDO line emission is dominated by warmer gas because of the line opacities. Indeed, even if the HDO abundance has a jump at $\sim$100 K, if the lines are optically thin than the warmer regions, with higher opacities may dominate the integrated intensity. One has also to consider that the water abundance has a further jump at around 220–250 K, caused by the reactions that convert all the gaseous atomic oxygen into water and that possess activation barriers making them efficient at $\geq$220 K (Ceccarelli, Hollenbach & Tielens 1996). The temperature is close to that derived from the LVG modelling, so that it is a plausible hypothesis that the gas probed by the observed HDO lines lies in a region warmer than the water desorption region because of the line opacities.

3.4 Water deuteration

Using the intensity 3σ upper limit of the para–$H_2^{18}O$ line at 203.407 52 GHz (see Section 3.1) and assuming a source size of 0.2 arcsec and a temperature of 200 K, we derive un upper limit to the $H_2^{18}O$ column density of $N(H_2^{18}O) \leq 8 \times 10^{17}$ cm^{-2}. Assuming the standard value of $^{16}O/^{18}O = 560$, the upper limit to the water column density is $N(H_2O) \simeq 4 \times 10^{20}$ cm^{-2}. Using the HDO column density previously derived, $N(HDO) = 4 \times 10^{17}$ cm^{-2}, leads to a lower limit to the water deuteration, $\geq 1 \times 10^{-3}$. Finally, using the derived n_{H_2} density (2×10^8 cm^{-3}) and emitting sizes (0.2 arcsec = 50 au in diameter) provides an estimate of the H_2 column density of $\sim$1.5 $\times$ 10^{23} cm^{-2} and, consequently of the HDO abundance of $\sim$3 $\times$ 10^{-6}. Similarly, the upper limit to the H_2O column density can be converted into an upper limit to the water abundance, namely $\leq 3 \times 10^{-3}$. We can, therefore, increase the real lower limit to the water deuteration considering that, reasonably, the water abundance cannot be larger than about $\sim$2 $\times$ 10^{-4}. This leads to a lower limit HDO/$H_2O \geq 0.015$.

This upper limit is consistent with those derived so far towards Class 0 protostars, $\sim$10^{-2} by Coutens et al. (2012) and Taquet et al. (2013), 0.3–8 $\times$ 10^{-2}, and larger than those quoted by Persson et al. (2013, 2014) and Coutens et al. (2013, 2014), 0.1–4 $\times$ 10^{-3}. Therefore, the deuteration of water does not seem to diminish from Class 0 to Class I sources. Yet, we conclude with a word of prudence, as this value of deuteration has been obtained taking the values of the LVG modelling. In particular, since the lines seem close to the LTE, the H_2 density could be larger and, consequently, the HDO abundance could be lower by the same factor.

4 CONCLUSIONS

The high sensitivity of the IRAM 30-m ASAI unbiased spectral survey in the mm-window allows us to detect towards the Class I object SVS13-A a large number of HDO emission lines with upper level energies up to $E_u = 837$ K. The non-LTE LVG analysis points to hot (150–260 K), dense ($\geq 3 \times 10^7$ cm^{-3}) gas associated with a quite small emitting region (50 au), supporting the occurrence of a hot corino inside SVS13-A. The HDO abundance is found to be $\sim$3 $\times$ 10^{-6}. Although the occurrence of shocks at such small

scales cannot be excluded, it is tempting to suggest we are observing for the first time the jump in the water abundance occurring at temperatures higher than 200 K, when the activation barriers of the gas phase reactions converting oxygen into water can be overcome.

Obviously, the final answer is in the hands of future interferometric observations [e.g. using Atacama Large Millimeter/submillimeter Array (ALMA)] imaging water emission around SVS13-A on scales $\leq$20 au.

REFERENCES

Altwegg K. et al., 2015, Science, 347, 387
Bachiller R., Guilloteau S., Gueth F., Tafalla M., Dutrey A., Codella C., Castets A., 1998, A&A, 339, L49
Busquet G. et al., 2014, A&A, 561, 120
Caselli P. et al., 2012, ApJ, 759, L37
Ceccarelli C., Hollenbach D. J., Tielens A. G. G. M., 1996, ApJ, 471, 400
Ceccarelli C. et al., 1999, A&A, 324, L21
Ceccarelli C., Castets A., Caux E., Hollenbach D., Loinard L., Molinari S., Tielens A. G. G. M., 2000, A&A, 355, 1129
Ceccarelli C., Maret S., Tielens A. G. G. M., Castets A., Caux E., 2003, A&A, 410, 587
Ceccarelli C., Caselli P., Herbst E., Tielens A. G. G. M., Caux E., 2007, in Reipurth B., Jewitt D., Keil K., eds, Protostars and Planets V. Univ. Arizona Press, Tucson, AZ, p. 47
Ceccarelli C., Caselli P., Bockelèe-Morvan D., Mousis O., Pizzarello S., Robert F., Semenov D., 2014, in Beuther H., Klessen R. S., Dullemond C. P., Henning T., eds, Protostars and Planets VI. Univ. Arizona Press, Tucson, AZ, p. 859

Chen X., Launhardt R., Henning Th., 2009, ApJ, 691, 1729
Codella C., Ceccarelli C., Nisini B., Bachiller R., Cernicharo J., Gueth F., Fuente A., Lefloch B., 2010, A&A, 522, L1
Codella C. et al., 2016, A&A, 586, L3
Coutens A. et al., 2012, A&A, 539, 132
Coutens A. et al., 2013, A&A, 560, A39
Coutens A., Jørgensen J. K., Persson M. V., van Dishoeck E. F., Vastel C., Taquet V., 2014, ApJ, 792, L5
Dubernet M.-L. et al., 2013, A&A, 553, 50
Eisner J. A., 2012, ApJ, 755, 23
Faure A., Wiesenfeld L., Scribano Y., Ceccarelli C., 2012, MNRAS, 420, 699
Herczeg G. J. S. et al., 2012, A&A, 540, 84
Hirota T. et al., 2008, PASJ, 60, 37
Karska A. et al., 2013, A&A, 552, 141
Kristensen L. E., Brown J. M., Wilner D., Salyk C., 2016, ApJ, 822, L20
Lee K. I. et al., 2016, ApJ, 820, L2
Lefloch B., Castets A., Cernicharo J., Langer W. D., Zylka R., 1998, A&A, 334, 269
Looney L. W., Mundy L. G., Welch W. J., 2000, ApJ, 529, 477
López-Sepulcre A. et al., 2015, MNRAS, 449, 2438
Persson M. V., Jørgensen J. K., van Dishoeck E. F., 2013, A&A, 549, L3
Persson M. V., Jørgensen J. K., van Dishoeck E. F., Harsono D., 2014, A&A, 563, 74
Pickett H. M., Poynter R. L., Cohen E. A., Delitsky M. L., Pearson J. C., Müller H. S. P., 1998, J. Quant. Spectrosc. Radiat. Transfer, 60, 883
Podio L. et al., 2012, A&A, 545, 44
Taquet V., López-Sepulcre A., Ceccarelli C., Neri R., Kahane C., Coutens A., Vastel C., 2013, ApJ, 768, L29
Tobin J. J. et al., 2016, ApJ, 818, 73
van Dishoeck E. F. et al., 2011, PASP, 123, 138
van Dishoeck E. F., Bergin E. A., Lis D. C., Lunine J. I., 2014, in Beuther H., Klessen R. S., Dullemond C. P., Henning T., eds, Protostars and Planets VI. Univ. Arizona Press, Tucson, AZ, p. 835
Willacy K. et al., 2015, Space Sci. Rev., 197, 151

This paper has been typeset from a TEX/LATEX file prepared by the author.